applied sciences

MDPI

Article

The Derivation of Vertical Damping Reduction Factors for the Design and Analysis of Structures Using Acceleration, Velocity, and Displacement Spectra

Aicha Rouabeh [1], Baizid Benahmed [1,*], Mehmet Palanci [2] and Issam Aouari [3]

[1] Development Laboratory in Mechanics and Materials, University of Djelfa, Djelfa 17000, Algeria; aicha.rouabeh@univ-djelfa.dz
[2] Civil Engineering Department, Istanbul Arel University, Istanbul 34220, Turkey; mehmetpalanci@arel.edu.tr
[3] Civil Engineering Department, Akli Mohand Oulhadj University, Bouira 10000, Algeria; i.aouari@univ-bouira.dz
* Correspondence: benahmed.tp@univ-djelfa.dz

Abstract: Damping reduction factors (DRFs) play a vital role in the seismic design of structures. DRFs have been widely studied due to their primary importance to the lateral resistance of structures subjected to earthquakes. On the other hand, devastating earthquakes have occurred all over the world, and recently, the Kahramanmaraş earthquakes in Turkey revealed the import of the vertical component of earthquakes and their impact on structures and infrastructures. Considering the importance of this parameter, this paper aims to develop new damping reduction factor (DRF) equations for the acceleration (DRFa), velocity (DRFv), and displacement spectra (DRFd) of the vertical components of earthquakes. For this purpose, 775 real ground motion records were selected from the Pacific Earthquake Engineering Research (PEER) strong motion database, and the vertical elastic response spectra of selected records were computed according to linear dynamic analysis. Taking the 5%-damped vertical response spectra as the target, the vertical spectral damping reduction factors (DRFa, DRFv, and DRFd) were computed for 1%, 3%, 10%, 15%, 20%, 30%, and 40% damping ratios. The effect of the earthquake magnitude, distance, and soil types on the DRFs was investigated. The results indicated that magnitude, distance, and soil type had no particular effect on the trend in the DRFs. Based on the evaluations, extensive statistical analyses were carried out, and new prediction equations were developed according to the nonlinear regression method. The developed equations were then compared to those found in the literature and seismic design codes. The comparisons proved that the proposed DRFa, DRFd, and DRFv models are strongly compatible with real DRFs and show strong robustness compared to existing models.

Keywords: damping reduction factor; vertical ground motion; vertical seismic response spectra; PEER database

check for updates

Citation: Rouabeh, A.; Benahmed, B.; Palanci, M.; Aouari, I. The Derivation of Vertical Damping Reduction Factors for the Design and Analysis of Structures Using Acceleration, Velocity, and Displacement Spectra. *Appl. Sci.* **2024**, *14*, 4348. https://doi.org/10.3390/app14114348

Academic Editor: Dario De Domenico

Received: 21 April 2024
Revised: 11 May 2024
Accepted: 13 May 2024
Published: 21 May 2024

1. Introduction

The effect of the vertical component of an earthquake on the response of structures was neglected for many years. Researchers, practitioners, and seismic codes (with some of these seismic codes being currently available) considered this component less noteworthy compared to the horizontal component. However, recently, some researchers have revealed the import of the vertical component, which may have a significant impact on structures and infrastructures. Strong vertical ground motions, for instance, may cause a significant increase in the axial forces on columns, the vertical displacement of beams [1], the vertical acceleration demands on the columns [2] in frames, and several important seismic demand parameters in highway bridges [3,4]. In addition, vertical components recorded far from faults can cause significant damage to buildings, as detailed by several researchers [5–7]. Therefore, a pertinent vertical design spectrum at different damping levels is required to assess the impacts of vertical ground motions on structures and to determine an acceptable structural design. On this subject, significant advancement has been achieved in recent decades.

According to studies conducted by various researchers [8–11] on the characteristics of the vertical response spectra using recorded ground motions, the vertical-to-horizontal response spectral ratio may surpass 2/3 for short periods. Currently, the vertical response spectra provided by many seismic design codes [12–15] and research publications [16] mainly consider a 5% damping ratio. However, a considerable number of structures with damping ratios different from 5% are vulnerable to vertical ground motion effects. Some long-cantilevered trusses [17], large-span spatial trusses [18], cold-formed steel floors [19], and composite floor decks [20] have damping ratios lower than 5%. On the other hand, structures with additional damping devices [21,22] and some types of steel structures with vertical hysteretic behavior [23,24] can exhibit a damping ratio greater than 5%.

To seismically design these structures to withstand vertical seismic actions at different damping ratios, the damping reduction factor (DRF) of the vertical response spectrum is required. In recent decades, few studies have been performed for the calculation of DRFs. Mohraz [25] used 54 recordings from 16 earthquakes to study the vertical response spectrum at five damping ratios, namely 0%, 2%, 5%, 10%, and 20%. Trifunac and Lee [26] used 438 ground motions from 104 earthquakes, mostly from California, to develop GMPEs using vertical pseudo-velocity response spectra at 0%, 2%, 5%, 10%, and 20% damping ratios. Other than California earthquakes, Berge-Thierry [27] adopted European vertical ground motions in their study and provided vertical pseudo-acceleration response spectra at damping ratios of 5%, 7%, 10%, and 20%. Later on, Malhotra [28] developed the acceleration constant, velocity constant, and displacement constant DRF functions for smooth vertical spectra. Rezaeian [29] developed a DRF model as a function of the damping ratios, natural periods, magnitude, and distance using 2229 vertical strong ground motion records of shallow crustal earthquakes in active tectonic regions from the Next Generation Attenuation-West2 database.

Akkar et al. [30] presented a damping model for scaling 5%-damped vertical spectral ordinates, and the model was based on a ground motion prediction equation for a vertical-to-horizontal spectral ratio [31] model developed for shallow active crustal regions in Europe and the Middle East. Xiang and Huang [32] considered the DRF for the absolute acceleration spectrum to be more susceptible to ground motion characteristics than the DRF for the pseudo-acceleration spectrum and presented a complex DRF model for the different acceleration spectra for different damping ratios and periods using 3198 vertical strong motion records on subduction earthquakes recorded by K-NET and KiK-net in Japan. Using 6466 vertical strong motion records on shallow crustal and upper-mantle earthquakes recorded by the Kyoshin network (K-NET) and the Kiban–Kyoshin network (KiK-net), Liu et al. [33] and Zhang and Chao [34] proposed site-related DRF models for the displacement spectra and the acceleration spectra, respectively. They concluded that magnitude and distance have a significant impact on the DRF according to their residual analysis.

Elhout [35] studied the influence of the closest distance, site conditions, earthquake magnitude, peak ground acceleration (PGA), and damping ratios on DRFs using 195 real vertical ground motion earthquakes selected from the PEER strong motion database. He indicated that the moment magnitude of an earthquake has a significant impact on DRFs, but the effect of the soil type, distance, and PGA is negligible. In addition, he developed simplified empirical formulations to compute the DRF for the vertical component. Hu et al. [36] employed 892 offshore and 4033 onshore ground motion records from the Kyoshin network to exhibit the differences in the DRFs of offshore and onshore ground motions. They stressed that the influence of the site conditions on offshore DRFs is extremely minor. They proposed offshore DRF models for horizontal and vertical acceleration spectra from Japan's Sagami Bay region based on 34 spectral periods and 10 damping ratios, where only the spectral periods and damping ratios were taken into account as variables. The uncertainty in the DRF model mainly depends on the path and site effects, and the standard deviations of the DRFs for the vertical component were slightly less than those for the horizontal component.

Recently, Çelik and Merter [37] presented the variation in the DRFa, DRFd, and DRFv in relation to the viscous damping ratio. The DRFs were computed by considering the displacement (Sd), pseudo-velocity (PSV), and pseudo-acceleration (PSa) response spectra. The mean DRF variations for a total of 20 real earthquake ground motions recorded in soft soil ($180 < V_{S30} \leq 360$ m/s) according to the Turkish Building Earthquake Code [15] were considered, and the records were selected from the NGA-West2 strong ground motion database. The authors found that for longer natural vibration periods (especially T > 1.0 s), the mean DRFs of the selected earthquake ground motions were nearly constant but fluctuated for T < 0.3 s. They ascertained that the mean DRF variations with respect to the viscous damping ratios were compatible with the code-based DRF relations for selected records. Sriwastav and Basu [38] used a set of 5962 records from the PEER NGA-West2 database. They explored the DRFv at 1%, 2%, 8% and 10% damping ratios with respect to 5% for a period range of 0–4.0 s. They stated that magnitude, epicentral distance, and soil type parameters are less practical and important to the DRFv. They proposed using a simplified relation as a function of the period to compute the DRFv regardless of the seismological parameters.

Based on the previous literature, existing studies have used local earthquakes, limited databases, or a specific response spectrum (i.e., acceleration, velocity, or displacement) to compute DRFs. For this reason, there is still a need to develop DRF models for the vertical component of earthquakes. The purpose of this study is to develop new DRF models for acceleration (DRFa), displacement (DRFd), and velocity (DRFv) response spectra considering 775 vertical ground motion records selected from active tectonic regions throughout the world. The response spectra of selected earthquakes corresponding to various damping ratios were computed to calculate the DRF values derived from the acceleration, displacement, and velocity response spectra. This database is a subset of the NGA-West2 database, which is part of a research program organized by the Pacific Earthquake Engineering Research Center (PEER). Three main equations are developed to predict the DRF values (DRFa, DRFd, and DRFv) and subsequently compared with those proposed in the literature and seismic codes in the latter part of this paper.

2. Calculation of Damping Reduction Factors

Damping reduction factors (DRFs) are essential for seismic design and the evaluation of structures. They are used to adjust the elastic response spectra for a 5% damping ratio to other higher or lower damping levels [39]. These factors are defined as follows [40]:

$$\mathrm{DRFa} = \frac{SA(\xi, \mathrm{T})}{SA(5\%, \mathrm{T})}, \mathrm{DRFv} = \frac{SV(\xi, \mathrm{T})}{SV(5\%, \mathrm{T})}, \mathrm{DRFd} = \frac{SD(\xi, \mathrm{T})}{SD(5\%, \mathrm{T})} \tag{1}$$

where $SA(\xi, \mathrm{T})$, $SV(\xi, \mathrm{T})$, and $SD(\xi, \mathrm{T})$, are the spectral accelerations, velocity, and displacement corresponding to a specific level of damping, respectively. The notations of $SA(5\%, \mathrm{T})$, $SV(5\%, \mathrm{T})$, and $SD(5\%, \mathrm{T})$ are the spectral accelerations, velocity, and displacement corresponding to 5% damping, respectively.

The first research to identify DRFs was carried out by Newmark and Hall [41], and this groundbreaking work highlighted that these factors rely upon the natural vibration period [42]. This study inspired scientists in this field, and afterward, DRFs were adopted in many seismic design codes. Table 1 shows the different DRF relationships for different design codes. In Figure 1, the code-based DRF relations determined using the equations given in Table 1 are presented based on different viscous damping ratios. The figure shows significant differences among the code-based period-independent DRF definitions. The lowest values for the DRFs have been suggested in the Japanese seismic design code. The great differences between the design codes imply the importance of studies on DRFs.

Table 1. Expressions for period-independent DRFs based on displacement response spectra defined in various design codes.

	Equation	Code Source	Reference
(1)	$\text{DRF} = \sqrt{10/(5+\xi)}$	Eurocode 8 (2004) Italian Code (2018)	[13] [43]
(2)	$\text{DRF} = 150/(100+10\xi)$	Japan JPN (2001)	[44]
(3)	$\text{DRF} = 1 + (5-\xi)/(6+1.4\xi)$	China (2010)	[14]
(4)	$\text{DRF} = (5.6 - \ln(\xi))/4$	ASCE/SEI (2014)	[12]
(5)	$\text{DRF} = (5/\xi)^{0.3}$	AASHTO (2010)	[45]
(6)	$\text{DRF} = \sqrt{7/(2+\xi)}$	Algerian RPA99 (2003)	[46]

Note: ξ should be taken as percentage, e.g., ξ = 10 for a damping ratio of 0.10.

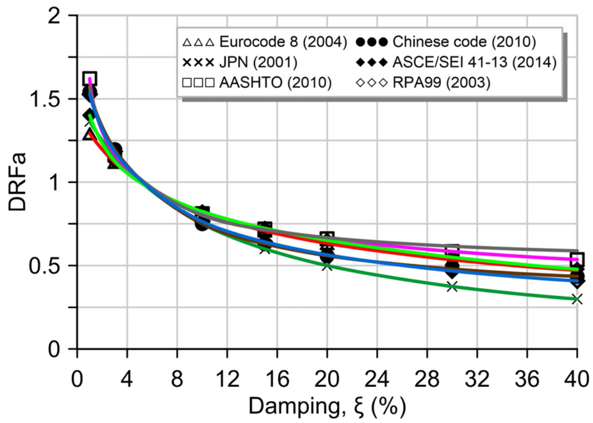

Figure 1. Damping reduction factors (DRFs) according to formulas proposed in seismic design codes [12–14,44–46].

3. Vertical Ground Motion Database

In this study, numerous real earthquake records, namely 775 vertical ground motion records, were selected from the PEER [47] strong motion database. The locations of the selected earthquakes are shown in Figure 2. A total of 171 earthquake events were considered to represent a wide range of site distances, average shear wave velocity (V_{S30}) intervals, and earthquake moment magnitudes (M_w). The moment magnitudes of the selected records range between 4.5 and 7.9, and their source-to-site distances (i.e., rupture distances R_{rup}) span up to 161.23 km. The site conditions of all the accelerograms are identified according to V_{S30} (the average shear wave velocity of the upper 30 m of the soil layer). The V_{S30} interval of the database is between 108.21 and 2016.13 m/s. Based on the V_{S30} intervals, selected ground motions were classified as A, B, C, and D regarding the site classification method given in Eurocode 8. Soil type A is rock or very stiff ($V_{S30} \geq 800$ m/s), soil type B is very dense sand or gravel or stiff clay (360 m/s $\leq V_{S30} < 800$ m/s), soil type C is dense or medium dense sand or gravel ($180 \leq V_{S30} < 360$ m/s), and soil type D is loose to medium cohesionless soil ($V_{S30} < 180$ m/s). The percentages of normal, reverse, and strike–slip events correspond to 21.05%, 30.4%, and 48.55% of the database, respectively.

The distribution of certain seismic features of selected earthquakes is presented in Figure 3. The number of events corresponding to different M_w, V_{S30}, and R_{rup} bins is given in Figure 3a–c. The distributions of M_w versus R_{rup} and M_w versus PGA are plotted in Figures 3d and 3e, respectively. It can be observed that the considered earthquakes are well distributed with respect to M_w, varying between 4.5 and 7.9. The PGA values of the selected strong motion records vary between 0.09 g and 0.35 g, which are also consistent with the minimum and maximum effective peak ground acceleration (EPGA) values, i.e., 0.05 g (corresponding to the design basis for earthquake hazards in areas of low seismicity) and 0.36 g (corresponding to the maximum considered earthquake hazard in high-seismicity areas), respectively, as recommended by several seismic design codes.

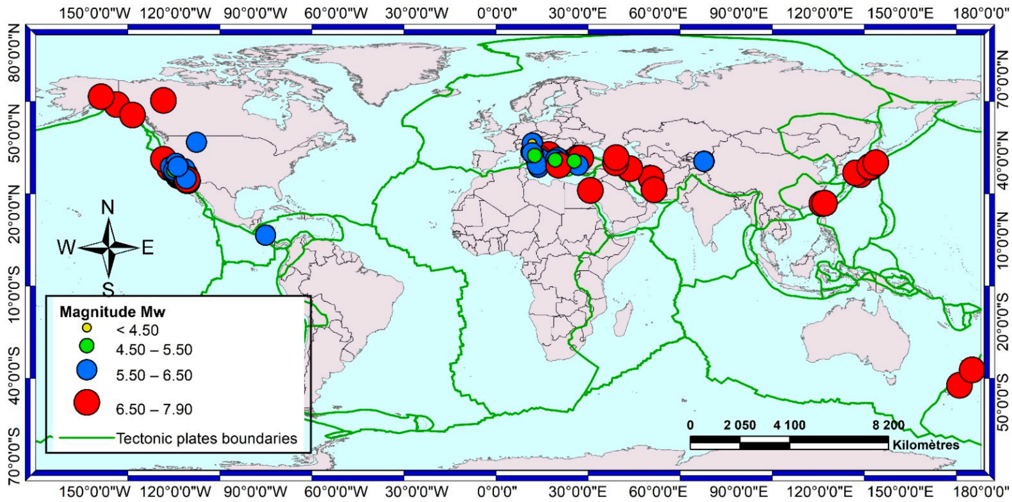

Figure 2. Localization of selected earthquakes for study database (source: developed maps).

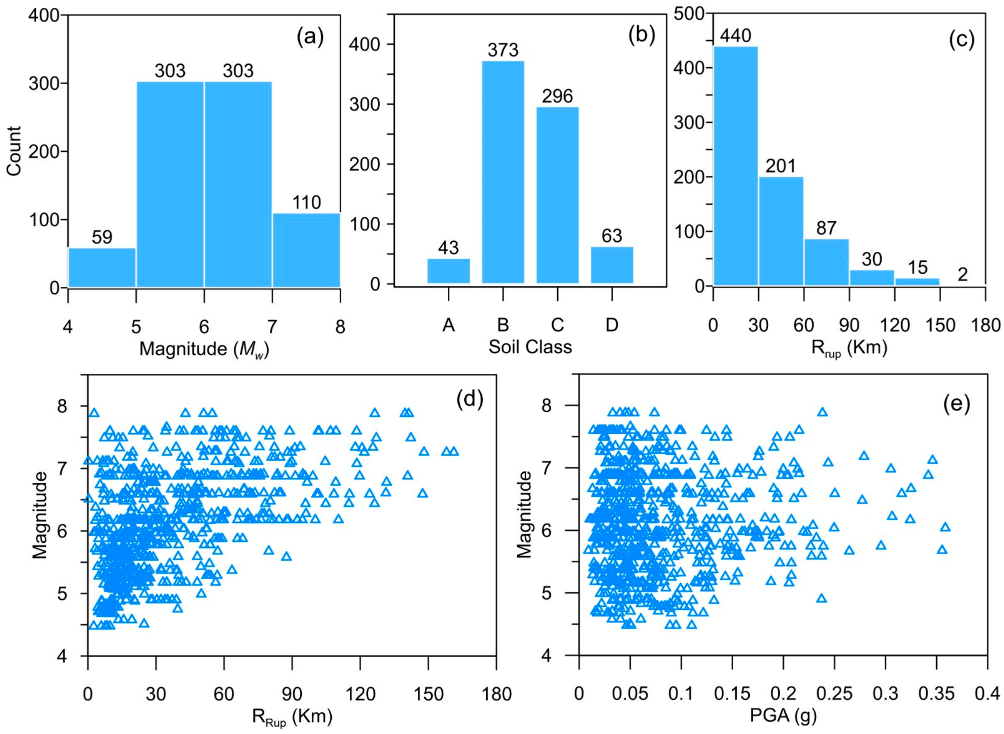

Figure 3. Database presentation: (**a**–**c**) data number according to seismic parameter range, (**d**) distribution of moment magnitude against rupture distance, (**e**) distribution of moment magnitude against PGA.

4. Effect of Seismic Parameters on Vertical DRFs

In this section, the effects of some important parameters such as the moment magnitude (M_w), the closest distance (R_{rup}), and the site conditions of the recorded accelerograms on the vertical DRFa, DRFd, and DRFv are discussed. The distribution of selected earthquakes in the database is plotted as a pie chart in Figure 4. In the study, the vertical ground motion spectra of the selected records are calculated at eight damping ratios (ξ) (1%, 3%, 5%, 10%, 15%, 20%, 30%, and 40%), and their mean DRFs are calculated for each of these parameters, namely M_w, R_{rup}, and V_{S30}. Then, the DRFs are computed for each damping ratio using Equation (1).

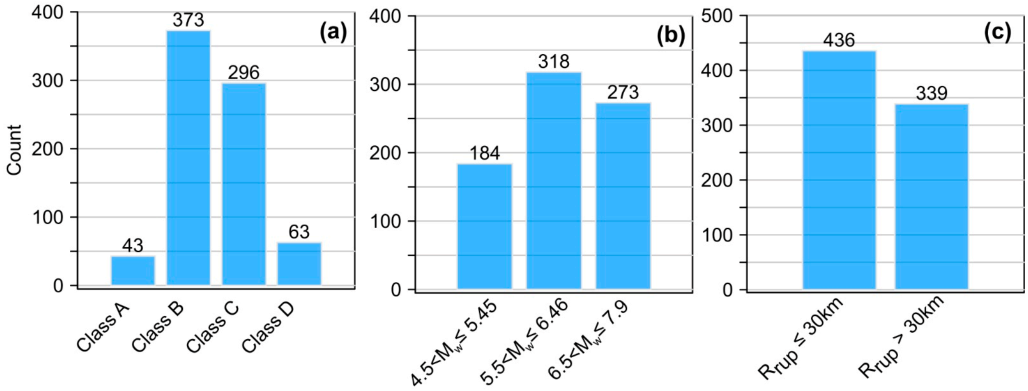

Figure 4. Distribution of (**a**) site classes, (**b**) earthquake magnitudes, and (**c**) rupture distances of the considered vertical ground motion records in the present study.

4.1. Effect of the Moment Magnitude

In this section, the vertical response spectra for each earthquake in each moment magnitude bin are calculated at different damping ratios, as seen in Figure 5. Later, the DRF values based on the acceleration, velocity, and displacement spectra are compared and evaluated for different earthquake magnitude bins.

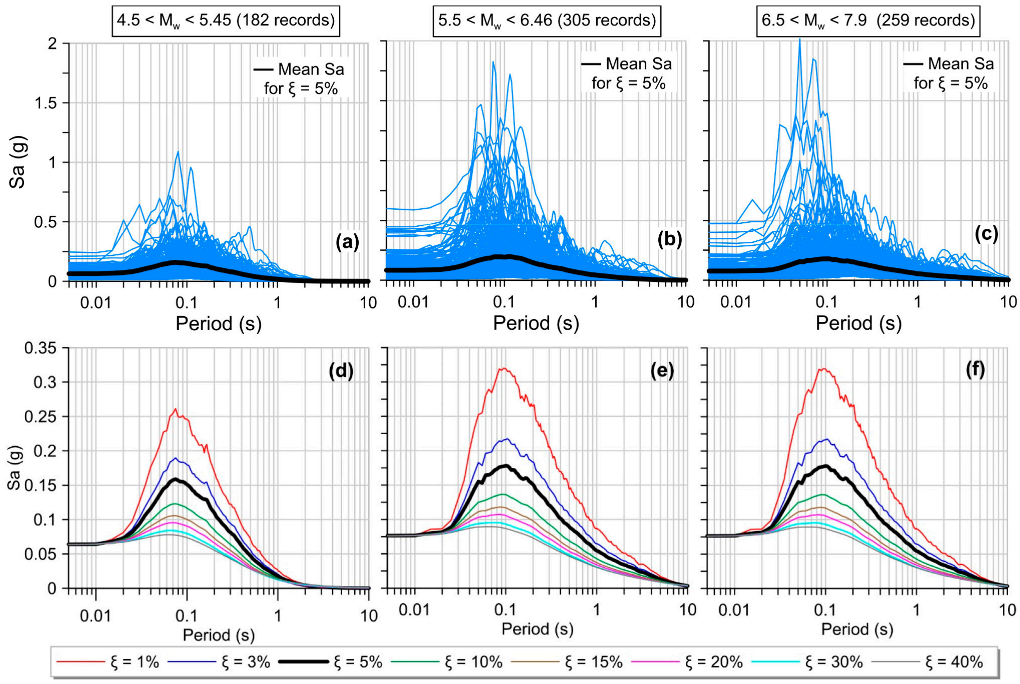

Figure 5. (**a**–**c**) Spectral acceleration spectra of selected earthquakes for different magnitude bins and $\zeta = 0.05$, (**d**–**f**) mean acceleration spectra calculated for different damping ratios.

Figure 6 shows the variation in the mean DRFs at damping ratios (ξ) equal to 1%, 3%, 10%, 15%, 20%, 30%, and 40% for the three moment magnitude bins ($4.5 \leq M_W \leq 5.45$, $5.5 \leq M_W \leq 6.46$, and $6.5 \leq M_W \leq 7.9$). It can be observed from Figure 6a–c that the effect of damping on the DRFa decreases at high magnitudes, especially for longer structural periods. It can be said that the variation in the DRFa values is almost the same for all the magnitude groups up to periods of 0.9 s, 0.7 s, 0.5 s, 0.4 s, and around 0.3 s at damping ratios of 10%, 15%, 20%, 30%, and 40%, respectively. After these periods, the DRFa values diverge, and it can be seen from the figures that the DRFa values for $4.5 \leq M_W \leq 5.45$ and $5.5 \leq M_W \leq 6.46$ are higher than those of $M_W \geq 6.5$. This situation is more pronounced with increasing damping and structural periods.

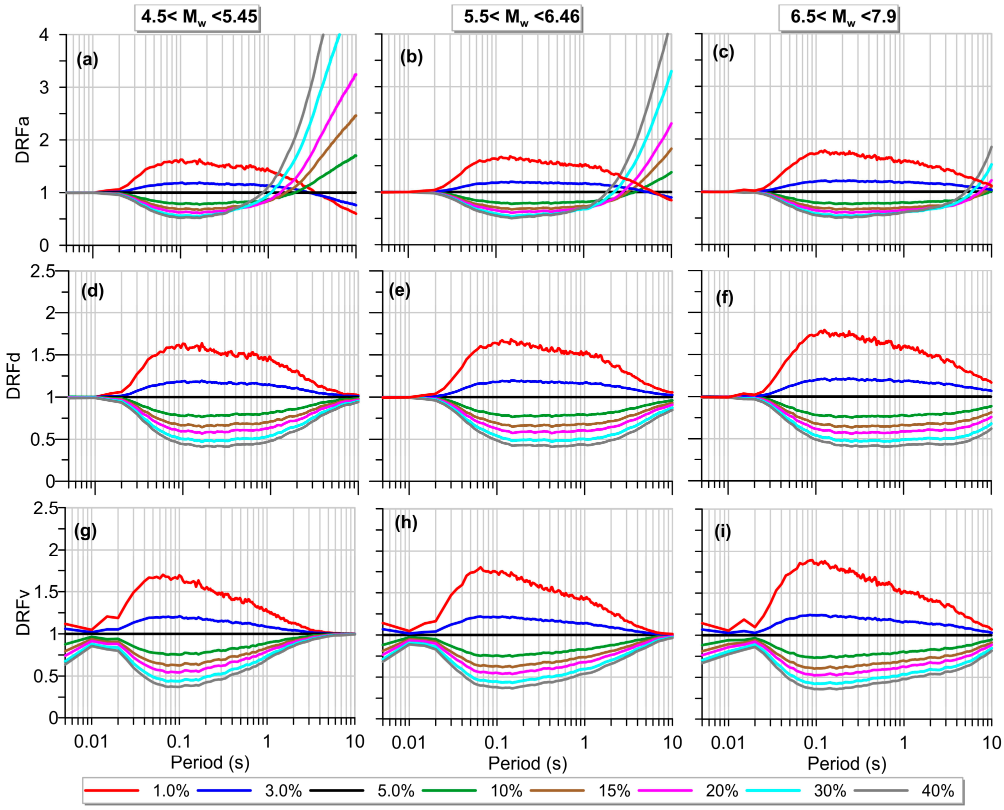

Figure 6. The variation in the median DRFs for different damping ratios and moment magnitudes; (**a**–**c**) DRFa, (**d**–**f**) DRFd, and (**g**–**i**) DRFv.

Figure 6d–f illustrates that the DRFd values are equal to unity for short periods (T < 0.02 s) and tend to diverge from unity with an increasing magnitude and longer periods. Figure 6g–i indicate that the DRFv curves are slightly different from the DRFa and DRFd curves, especially for short periods, and the DRFv values approach unity at T < 0.02 s. Then, the DRFv values diverge from unity with an increasing duration until 0.1 s. After a 1.0 s period, the DRFv values approach unity again, especially for low moment magnitudes $M_W \leq 6.5$.

In Figure 7, the distributions of the DRFa, DRFv, and DRFd values for the three different magnitude bins are compared against the structural periods. It can be seen from Figure 7 that the DRFd and DRFv curves are almost identical and higher than unity for all the magnitude groups at low damping ratios (i.e., 1.0% and 3.0%). The DRFd and DRFv values are lower than unity at high damping ratios (ξ > 5%) and move away from unity with increasing damping ratios.

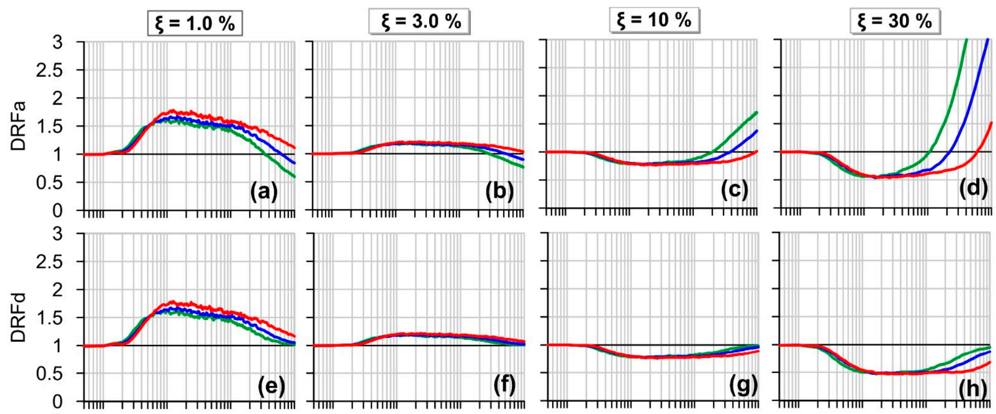

Figure 7. *Cont.*

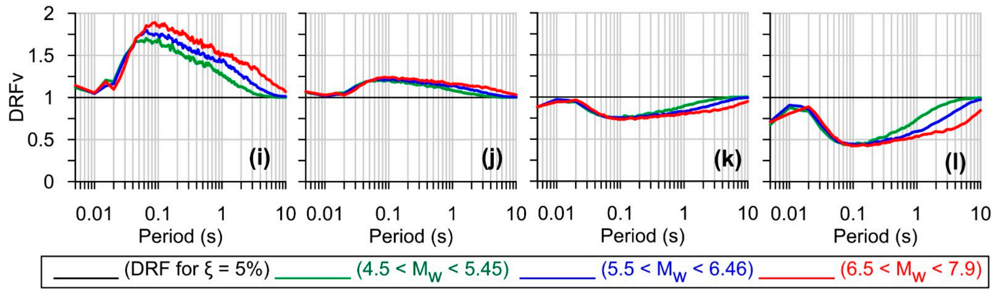

Figure 7. Effect of moment magnitude (M_w) on DRFs calculated for different damping ratios; (**a**–**d**) DRFa, (**e**–**h**) DRFd, and (**i**–**l**) DRFv.

Similar observations can be also made for the DRFa values, except for those corresponding the moderate-length to long structural periods. For example, the DRFa values are higher than unity at damping ratios of 1% and 3%, but these values may be below unity at low magnitudes ($M_w < 6.5$) and for long structural periods (T > 1.0 s). Also, the DRFa values are lower than unity at high damping ratios (ξ > 5%), but the DRFa values can be increased by 3 times or more for structural periods (T > 1.0 s). In general, at low damping ratios (i.e., 1.0% and 3.0), a greater M_w will result in greater DRFs. This situation is reversed at high damping ratios (ξ > 5%), and this trend has also been observed by various researchers [29,32,35,48,49].

4.2. The Effect of Distance

Figure 8 shows the variation in the mean DRFs at damping ratios (ξ) equal to 1%, 3%, 10%, 15%, 20%, 30%, and 40% for two source–site distance groups. The first group corresponds to less than 30 km, and the other is higher than 30 km.

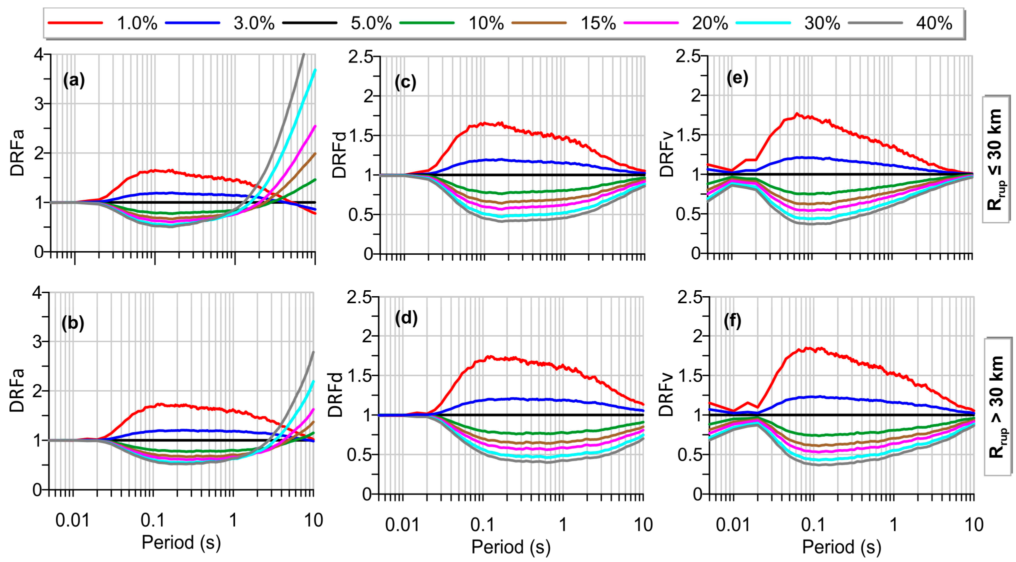

Figure 8. The variation in the median DRFs for different damping ratios by rupture distance; (**a**,**c**,**e**) $R_{rup} \leq 30$ km, (**b**,**d**,**f**) $R_{rup} > 30$ km.

Figure 8 shows that the DRFa is less sensitive to the damping ratio at a distance higher than 30 km compared to the DRFd and DRFv. Figure 8c,d show that the DRFd is equal to unity for very short period values, and it tends to move away from unity as the rupture distance increases for long ranges of structural periods. This tendency is consistent with the studies carried out by Rezaeian et al. [29]. The results in Figure 8e,f indicate that the DRFv curves approach unity, especially for short periods (T < 0.02 s). Then, the DRFv values diverge from unity until reaching 0.1 s. After 1.0 s, the DRFv values approach unity again for long structural periods and $R_{rup} \leq 30$ km.

In Figure 9, the difference between the DRF curves of the distinct distance bins (i.e., $R_{rup} \leq 30$ and $R_{rup} > 30$ km) is compared at different damping ratios. The figure indicates that the DRFa values are almost the same for all the distance groups up to periods of 0.02 s, 1.5 s, 0.9 s, 0.7 s, 0.5 s, 0.4 s, and around 0.3 s for damping ratios of 1%, 3%, 10%, 15%, 20%, 30%, and 40%, respectively. Beyond these periods, the differences become more evident at high damping and for longer periods.

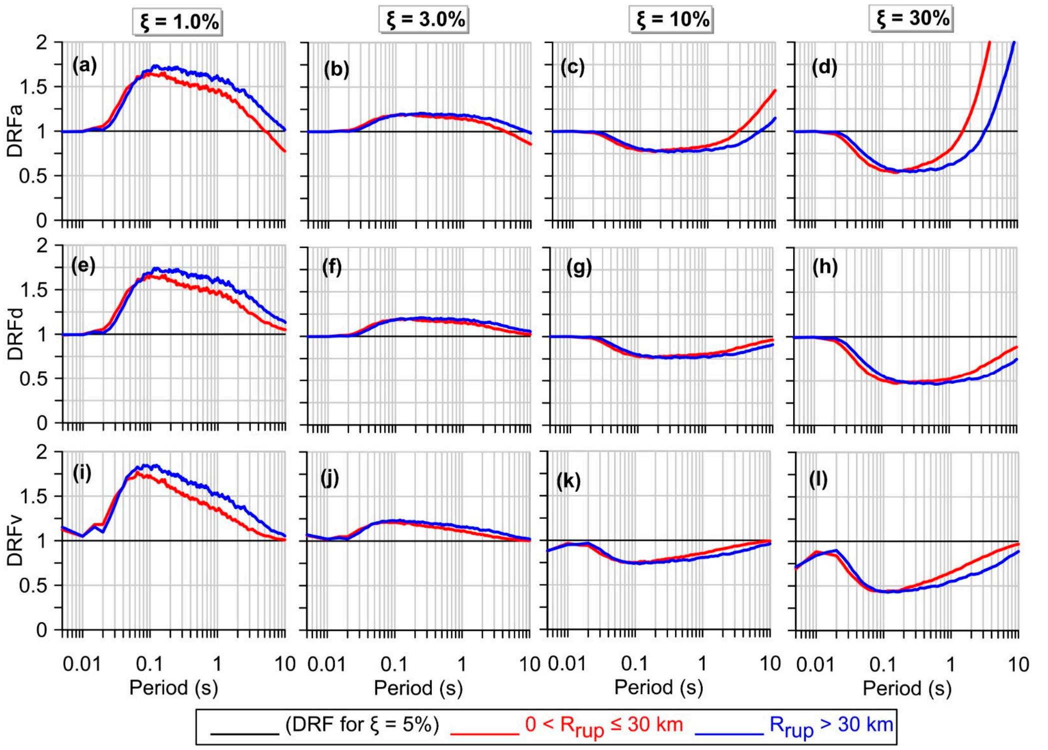

Figure 9. Effect of rupture distance (R_{rup}) on DRFs; (**a**–**d**) DRFa, (**e**–**h**) DRFd, and (**i**–**l**) DRFv.

The figures for the DRFd (see Figure 9e–h) and the figures for the DRFv (see Figure 9i–l) clearly indicate that the DRF values are greater than unity at damping ratios lower than 5% and lower than unity under the opposite conditions for both of these types of DRFs. It can be also said that the DRFs calculated for $R_{rup} > 30$ km are higher than the DRFs calculated for $R_{rup} < 30$ km in general. This difference becomes more pronounced as the damping and the structural period increase. This trend has also been observed by Xiang and Huang [32]. In general, it can be considered that the DRFd and DRFv are not influenced by the rupture distance parameter.

4.3. Effect of the Site Conditions on the Vertical DRFs

Figure 10 illustrates the mean DRF curves of distinct soil classes (i.e., A, B, C, and D) at damping ratios (ξ) equal to 1%, 3%, 10%, 15%, 20%, 30%, and 40%. The results presented in the figure show that the amplitude of and trend in the DRFs are relatively similar for site classes A and D, as also observed by Elhout [35]. In addition, the same tendency for soil classes B and C is also observed in the DFRa values. It can be also observed from the figures that the DRFa and DRFd curves follow a fairly similar path, and the DRFs are very close to unity for periods lower than 0.02 s ($T < 0.02$ s) and for all soil classes. On the other hand, the DRFd and DRFv curves are almost identical for periods longer than 1.0 s ($T > 1.0$ s) and tend to decrease, almost reaching unity with an increasing natural period. From very short periods to 0.02 s, the DRFv values become narrow and very close to unity for all the soil classes.

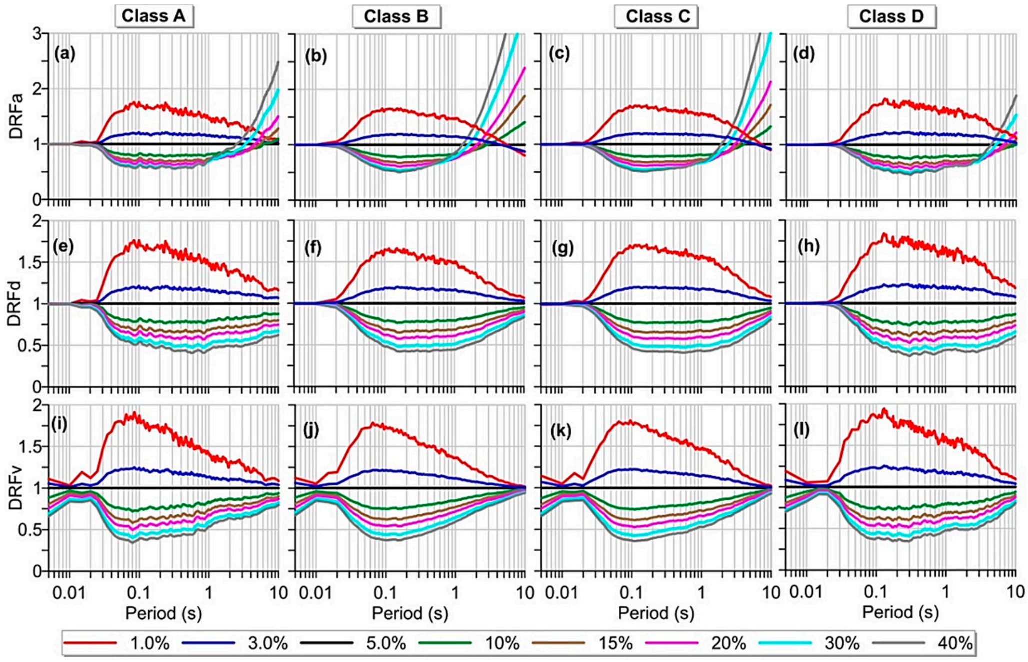

Figure 10. The variation in the median DRFs for different damping ratios by site conditions; (**a**–**d**) DRFa, (**e**–**h**) DRFd, and (**i**–**l**) DRFv.

A comparison of the DRF values for distinct soil classes is plotted in Figure 11 for different damping ratios. It can be said that the DRF values have no specific order and follow no systematic path for distinct soil classes. For example, the DRFs calculated from the earthquakes recorded in soil A are slightly greater than those for the ground motions recorded in soil type D, and the DRFs calculated from the earthquakes recorded in soil type B are slightly greater than those for the ground motions recorded in soil type C. It is noticeable that the DRFa values are very close to each other for the different soil classes and at damping ratios of 1% and 3% according to Figure 11a–d. However, the differences become more evident for periods longer than 1.0 s (T > 1.0 s) at almost all the damping ratios (especially for $\xi > 1\%$). Based on these results, it can be highlighted that soil type has no apparent effect on the DRFa at low damping ratios, and the effect of soil type seems to be evident for periods longer than 1.0 s at high damping ratios. Except for small differences at shorter periods (T < 0.02 s), the trends in the DRFd and DRFv curves are almost identical, especially compared to that of the DRFa. In general, the results indicate that the soil type has no apparent effect on the DRFd or the DRFv. This conclusion is also consistent with the results reported by various researchers in the literature [28,29,32,33,50].

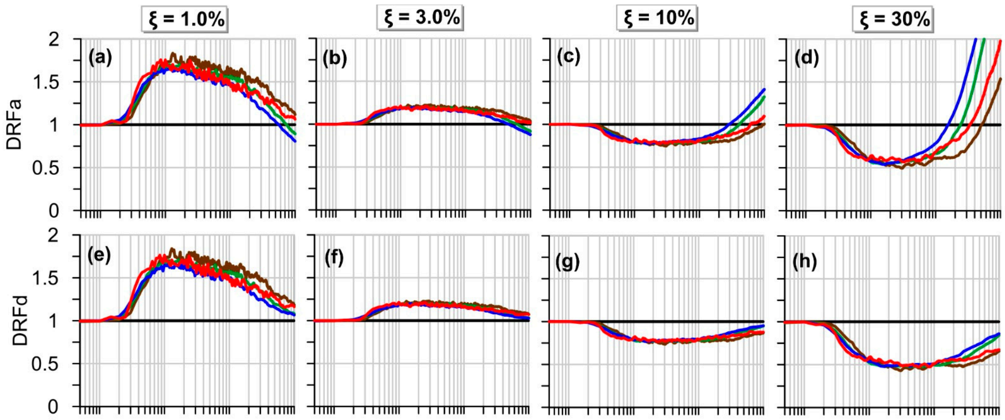

Figure 11. *Cont.*

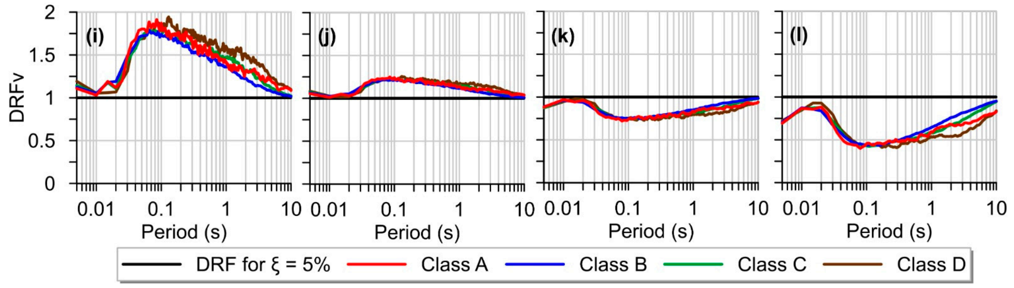

Figure 11. Effect of site conditions on DRFs; (**a**–**d**) DRFa, (**e**–**h**) DRFd, and (**i**–**l**) DRFv.

5. A New Prediction Model for Vertical DRFs

To understand the general features of and to provide the best estimate of the DRFs for the vertical component of ground motions, the mean DRFs are computed and compared for different damping ratios regardless of the seismic parameters (see Figure 12). According to Figure 12, the mean DRFa and DRFd values are close to each other at low damping ratios ($\xi < 10\%$), but significant differences can be observed for damping ratios greater than 10% for all the period ranges. Differences evidently appear around periods of 1 s, 0.6 s, 0.2 s, 0.1 s, and 0.005 s at damping ratios of 10%, 15%, 20%, 30%, and 40%, respectively. Although some differences can be noted at around 3.0 s at low damping ratios of 1% and 3%, these differences are minor and can be neglected. From very short periods to 0.02 s, the DRFv values become narrow and approach unity, and the trend in the DRFv is different from those of the DRFa and DRFd in this respect. Compared to the DRFv and DRFd values, the DRFa values increase dramatically with an increasing period at a damping ratio greater than 10%. Moreover, the DRFd and DRFv are less sensitive to the period and damping ratio than the DRFa. Based on the above results, it can be said that different mathematical equations should be proposed to obtain the best predictions for the DRFa, DRFv, and DRFd values.

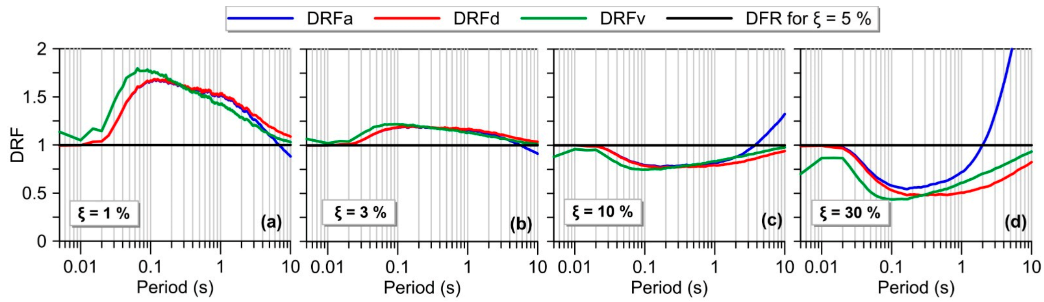

Figure 12. Comparison between mean DRFs obtained from acceleration spectra (DRFa), displacement spectra (DRFd), and velocity spectra (DRFv) at different damping ratios; (**a**) $\xi = 1\%$, (**b**) $\xi = 3\%$, (**c**) $\xi = 10\%$, and (**d**) $\xi = 30\%$.

In the next step, new period-dependent equations are developed to characterize the mean damping reduction factors for the selected earthquakes. The matching of the predicted and computed DRF values is used as a criterion, and the correlation between the predicted and computed DRFs is evaluated. In addition, coefficient of determination (R^2), Sum of Squares for Error (SSE), and Root Mean Square Error (RMSE) values are used to determine the efficiency of the proposed equations. Nonlinear regression is used to analyze the complex relations between the dependent and independent variables [51,52], used here to obtain the best fit. This operation is performed using the Levenberg–Marquardt algorithm, used as a standard technique to solve nonlinear least-squares problems. After several trials, Equations (2)–(4) are proposed to approximate the DRFs (DRFa, DRFd and DRFv). It is noted that the obtained equations present a high correlation with real DRF values.

5.1. Nonlinear Regression of the Mean DRFs of All the Selected Ground Motions

Based on several studies [32,33,35,36] and the observations in this study, the polynomial function of natural logarithms of the natural vibration period and damping ratio parameters can be used to describe the relations of the DRFs.

Considering the theoretical boundary constraints of the DRF with respect to the natural vibration period, the DRF tends to approach unity when the natural vibration period is close to zero or infinity. The proposed functions for predicting the acceleration, displacement, and velocity DRFs are expressed by Equations (2)–(4), respectively.

$$\mathrm{DRFa} = \mathrm{a_0} + \mathrm{a_1}\cos(\mathrm{T}\times\mathrm{w}) + \mathrm{b_1}\sin(\mathrm{T}\times\mathrm{w}) + \mathrm{a_2}\cos(2\times\mathrm{T}\times\mathrm{w}) + \mathrm{b_2}\sin(2\times\mathrm{T}\times\mathrm{w}) \tag{2}$$

$$\mathrm{DRFd} = \mathrm{a_0} + \mathrm{a_1}\cos(\mathrm{T}\times\mathrm{w}) + \mathrm{b_1}\sin(\mathrm{T}\times\mathrm{w}) + \mathrm{a_2}\cos(2\times\mathrm{T}\times\mathrm{w}) + \mathrm{b_2}\sin(2\times\mathrm{T}\times\mathrm{w}) \tag{3}$$

$$\mathrm{DRFv} = \begin{cases} \mathrm{a_0} + \mathrm{a_1}\cos(\mathrm{T}\times\mathrm{w}) + \mathrm{b_1}\sin(\mathrm{T}\times\mathrm{w}) + \mathrm{a_2}\cos(2\times\mathrm{T}\times\mathrm{w}) + \mathrm{b_2}\sin(2\times\mathrm{T}\times\mathrm{w}), & \text{For T} < 0.10\ \mathrm{s} \\ \mathrm{a}\times\mathrm{T^b} + \mathrm{c}, & \text{For T} \geq 0.10\ \mathrm{s} \end{cases} \tag{4}$$

Tables 2–4 show the values of the fitting coefficients for the prediction of the mean DRFs. The R^2 between the calculated and predicted mean DRFs for the database is greater than 0.99. The RMSE is predominantly less than 0.02 and, reaching a maximum value of 0.065, is very low, still implying strong correlation and low error. In addition, the SSE values are also given in the corresponding tables for comparison of each model. According to the calculations, the SSE ranges around 0.001–0.089, 0–0.09, and 0–0.329 for the DRFa, DRFd, and DRFv, respectively. It seems that the SSE is slightly higher, resulting from the simplified equation, for $T \geq 0.10$ s. Nevertheless, the R^2 is higher than 0.993, and the RMSE is quite low and equal to 0.013, which implies the accuracy of the equation. Based on these statistical results, it can be said that the proposed DRF models can capture the main features of the DRFs as a function of the vibration period and the damping ratio.

A comparison of the prediction of the proposed DRF models with the real mean values of the DRFs is given in Figure 13, and the figure clearly presents the prediction accuracy of the proposed equations. Despite the small differences between the real and predicted values for very short periods (T < 0.03 s), it is apparent that the proposed DRF models have a strong robustness and accuracy.

Table 2. Coefficients and quality regression of the mean DRFa constructed from acceleration spectra.

		1%	3%	10%	15%	20%	30%	40%
For T > 0.15 s	a_0	1.438	1.049	1.376	1.382	1.597	2.086	2.633
	a_1	0.320	0.146	−0.547	−0.647	−0.917	−1.462	−2.035
	b_1	−0.581	−0.068	−0.182	−0.034	0.001	0.083	0.180
	a_2	−0.110	−0.003	−0.051	−0.065	−0.079	−0.102	−0.120
	b_2	−0.058	−0.025	0.164	0.123	0.164	0.256	0.363
	w	0.207	0.251	0.192	0.244	0.248	0.250	0.245
	SSE	0.089	0.008	0.005	0.009	0.016	0.027	0.037
	R^2	0.999	0.999	1.000	1.000	1.000	0.999	0.999
	RMSE	0.007	0.002	0.002	0.002	0.003	0.0037	0.004
For T ≤ 0.15 s	a_0	1.430	1.119	0.867	0.805	0.767	0.725	0.703
	a_1	−0.332	−0.093	0.104	0.152	0.180	0.211	0.229
	b_1	−0.048	−0.018	0.020	0.032	0.039	0.045	0.044
	a_2	−0.112	−0.029	0.032	0.046	0.056	0.066	0.071
	b_2	−0.014	−0.004	0.003	0.004	0.004	0.005	0.004
	w	30.030	29.970	28.620	28.800	28.830	28.890	28.860
	SSE	0.010	0.001	0.001	0.001	0.002	0.002	0.003
	R^2	0.995	0.996	0.996	0.997	0.997	0.997	0.997
	RMSE	0.020	0.005	0.005	0.007	0.008	0.010	0.010

Table 3. Coefficients and quality regression of the mean DRFd constructed from displacement spectra.

		1%	3%	10%	15%	20%	30%	40%
For T < 0.15 s	a_0	1.432	1.120	0.863	0.795	0.751	0.696	0.661
	a_1	−0.332	−0.093	0.107	0.159	0.192	0.234	0.263
	b_1	−0.063	−0.023	0.025	0.039	0.047	0.053	0.051
	a_2	−0.109	−0.029	0.032	0.047	0.057	0.070	0.078
	b_2	−0.020	−0.006	0.004	0.005	0.004	0.002	−0.002
	w	31.300	31.500	30.000	29.920	29.760	29.560	29.210
	SSE	0.008	0.000	0.001	0.001	0.002	0.002	0.002
	R^2	0.995	0.997	0.997	0.997	0.998	0.998	0.998
	RMSE	0.019	0.004	0.005	0.007	0.008	0.009	0.010
For T ≥ 0.15 s	a_0	1.792	1.128	0.857	0.814	874,200	1,915,000	0.627
	a_1	0.058	0.074	−0.090	−0.165	−1,165,000	−2,553,000	−0.217
	b_1	−0.888	−0.077	0.048	0.049	26,320	50,080	0.064
	a_2	−0.193	−0.008	0.000	−0.002	26,320	638,000	−0.006
	b_2	0.007	−0.018	0.019	0.046	−13,160	−25,050	0.042
	w	0.169	0.252	0.252	0.210	−0.004	−0.004	0.241
	SSE	0.090	0.007	0.004	0.007	0.009	0.013	0.016
	R^2	0.998	0.998	0.999	0.999	0.999	0.999	0.999
	RMSE	0.007	0.002	0.001	0.002	0.002	0.003	0.003

Table 4. Coefficients and quality regression of the mean DRFv constructed from velocity spectra.

		1%	3%	10%	15%	20%	30%	40%
For T < 0.1 s	a_0	1.493	1.138	0.837	0.766	0.667	0.654	0.616
	a_1	−0.382	−0.108	0.122	0.186	0.246	0.277	0.309
	b_1	−0.042	0.001	0.003	0.013	−0.012	−0.007	−0.027
	a_2	−0.104	−0.029	0.034	0.046	0.077	0.066	0.072
	b_2	−0.019	0.002	−0.004	−0.002	−0.061	−0.015	−0.026
	w	43.070	38.370	36.160	39.780	27.400	38.260	37.460
	SSE	0.010	0.000	0.001	0.001	0.002	0.002	0.002
	R^2	0.993	0.998	0.993	0.996	0.995	0.997	0.997
	RMSE	0.027	0.004	0.009	0.010	0.013	0.012	0.013
For T ≥ 0.1 s	a	9.503	−0.696	0.392	0.512	0.581	0.669	0.728
	b	−0.018	0.070	0.138	0.156	0.165	0.173	0.176
	c	−8.100	1.825	0.444	0.237	0.109	−0.057	−0.166
	SSE	0.329	0.022	0.014	0.023	0.027	0.035	0.044
	R^2	0.993	0.995	0.998	0.998	0.999	0.999	0.999
	RMSE	0.013	0.003	0.003	0.003	0.004	0.004	0.005

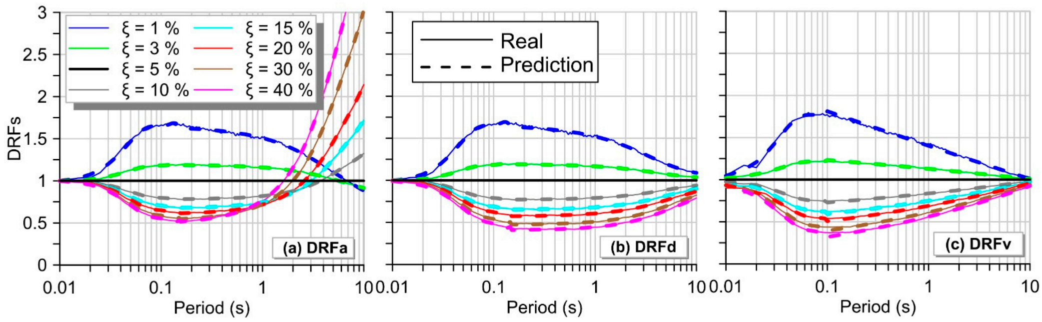

Figure 13. The real mean DRF curves vs. the proposed ones given by Equations (2)–(4) for different damping ratios; (**a**) DRFa, (**b**) DRFd, and (**c**) DRFv.

5.2. Comparison of the Models

Several DRF prediction models have been suggested in the literature, as discussed in the introduction. However, the accuracy of these models is dependent on multiple factors, such as the database considered, the limitations of the analysis models, and the use of different vertical spectra. To illustrate the accuracy of the proposed model, some of the published models are used for comparison. Since the proposed vertical DRF models considered in this study are derived for the acceleration, displacement, and velocity spectra, existing predictive models given in Table 5 used for distinct vertical response spectra are considered. Figure 14 shows a comparison of the mean DRFa values of the proposed model with those of existing models from the literature at damping ratios of 2%, 3%, 10%, 20%, 30%, and 40%. It can be noted from the figure that the existing DRFa models may have different predictions at various damping ratios. According to the database of the Lin and Chang model, the effect of the damping ratio was also not obvious since all the DRF values were almost identical at a damping ratio lower than 5%, and the model was developed for $T \geq 0.1$ s. For this reason, Lin and Chang's model completely differs from the other models when the damping ratio is less than 10%. Except for the Lin and Chang model, the proposed model and the existing models yield similar results with relatively small differences at $\xi \leq 10\%$. The predicted DRFa curves have a similar pattern when the damping ratio is higher than 10%. On the other hand, the predictions of the models separated and thus the differences between the models increased when the damping ratio was higher than 10%. The proposed model has the highest accuracy at all damping ratios and for all period ranges, compared to the existing models.

Table 5. The considered DRFs proposed in the literature for comparison.

		Equation	Ref.	Limit Condition
DRFa	(1)	$\mathrm{DRFa} = \begin{cases} a_1\log(T)^2 + b_1\log(T) + c_1 & 0.03 \leq T \leq 0.12\ \mathrm{s} \\ a_2 + b_2\cos(f_2\log(T)) + c_2\sin(f_2\log(T)) & 0.12 \leq T \leq 10.0\ \mathrm{s} \\ +d_2\cos(2f_2\log(T)) + e_2\sin(2f_2\log(T)) & \end{cases}$	[32]	
	(2)	$\mathrm{DRFa} = \begin{cases} 1, & T \leq 0.02\ \mathrm{s} \\ c_1 + c_2e^{c_3T}, & 0.02\ \mathrm{s} < T \leq 0.2\ \mathrm{s} \\ c_1 + c_4T, & T > 0.2\ \mathrm{s} \end{cases}$	[38]	For ξ = 1, 2, 8, 10% Vertical spectra only
	(3)	$\mathrm{DRFa}(T,\xi) = 0.342\xi^{-0.354} + (0.0186 + 0.368\xi - \frac{1}{10.644\xi^2})T$	[53]	
	(4)	$\mathrm{DRFa}(T,\xi) = \begin{cases} 1 - \frac{aT^b}{(T+1)^c}, & \xi < 0.05 \\ d + eT, & \xi > 0.05 \end{cases}$	[54]	$0.01\ \mathrm{s} < T \leq 4\ \mathrm{s}$ $0.005 < \xi \leq 0.5$
DRFd	(5)	$\mathrm{DRFd}(T,\xi) = 1 - \frac{aT^b}{(T+1)^c}$	[54]	$0.01\ \mathrm{s} < T \leq 4\ \mathrm{s}$ $0.005 < \xi \leq 0.5$
	(6)	$\mathrm{DRFd}(T,\xi) = 1 + (\xi - 0.05)\left(1 + a_1\ln\xi + a_2(\ln\xi)^2\right) \times \left(a_3 + a_4\ln T + a_5(\ln T)^2\right)$	[40]	$0.1\ \mathrm{s} < T \leq 5\ \mathrm{s}$ $0.005 < \xi \leq 0.5$
	(7)	$\mathrm{DRFd}(T,\xi) = 0.582 + 0.418 \times (12.279 - T)^{-3.9\times(\xi-0.05)}$	[55]	$0.1\ \mathrm{s} < T \leq 10\ \mathrm{s}$ $0.05 < \xi \leq 0.25$
	(8)	$\mathrm{DRFd}(T,\xi) = \begin{cases} \frac{1}{\left(1-f(\xi)\frac{T^{8.76}}{(T+0.01)^{8.94}}\right)} \\ f(\xi) = -0.031\ln\left(\frac{\xi}{5}\right)^2 + 0.386\ln\left(\frac{\xi}{5}\right) \end{cases}$	[56]	
DRFv	(9)	$\mathrm{DRFv}(T,\xi) = 1 + A/\left(B(\ln T)^4 + C(\ln T)^3 + D(\ln)^2 + E(\ln T) + 1\right)$	[33]	$0.1\ \mathrm{s} < T \leq 10\ \mathrm{s}$ $0.01 < \xi \leq 0.25$
	(10)	$\mathrm{DRFv}(T,\xi) = 1 + (\xi - 0.05)\left(1 + a_1\ln\xi + a_2(\ln\xi)^2\right) \times \left(a_3 + a_4\ln T + a_5(\ln T)^2\right)$	[40]	

In Figure 15, DRFd predictive models from various studies [40,54–56] are compared with the developed model at damping ratios of 1%, 3%, 10%, 20%, 30%, and 40%. In general, all the models have similar trends for distinct period ranges. Due to its limited number of ground motion records and its consideration of the Algerian code in terms of the soil classification and the response spectrum [46], the Benahmed model differs from all the other models. The differences between the existing models change depending on the damping ratios and the period range. There is no apparent harmony between the existing models and the proposed model, especially at 1% damping. However, the proposed model has very good agreement with the mean DRFd ratios determined from the analysis. Except for at 1% damping, the Saez model has good compatibility with the proposed model for the DRFd.

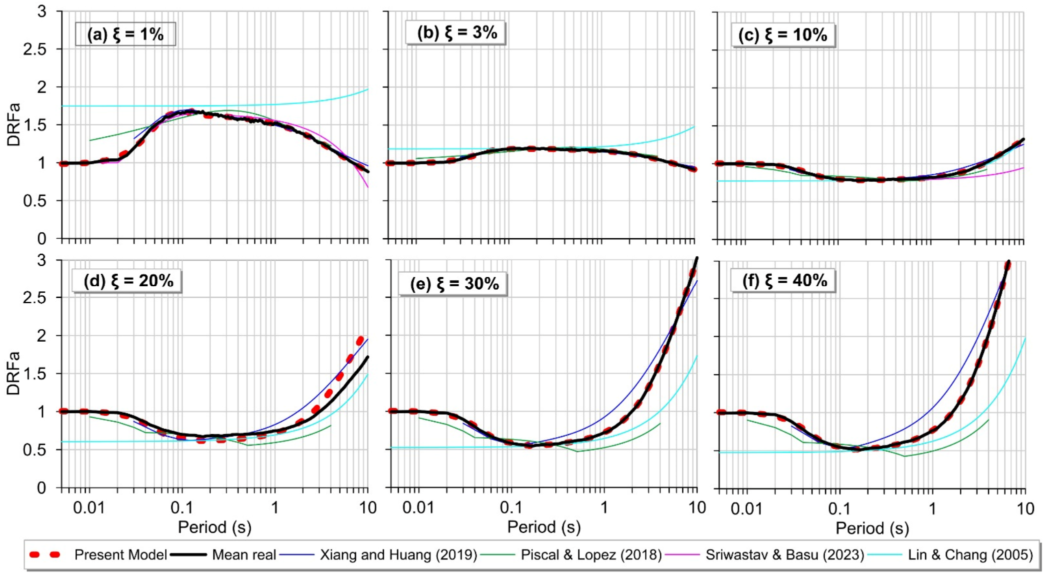

Figure 14. Comparison of proposed DRFa with equations given in Table 5 [32,50,53,54] for different damping values.

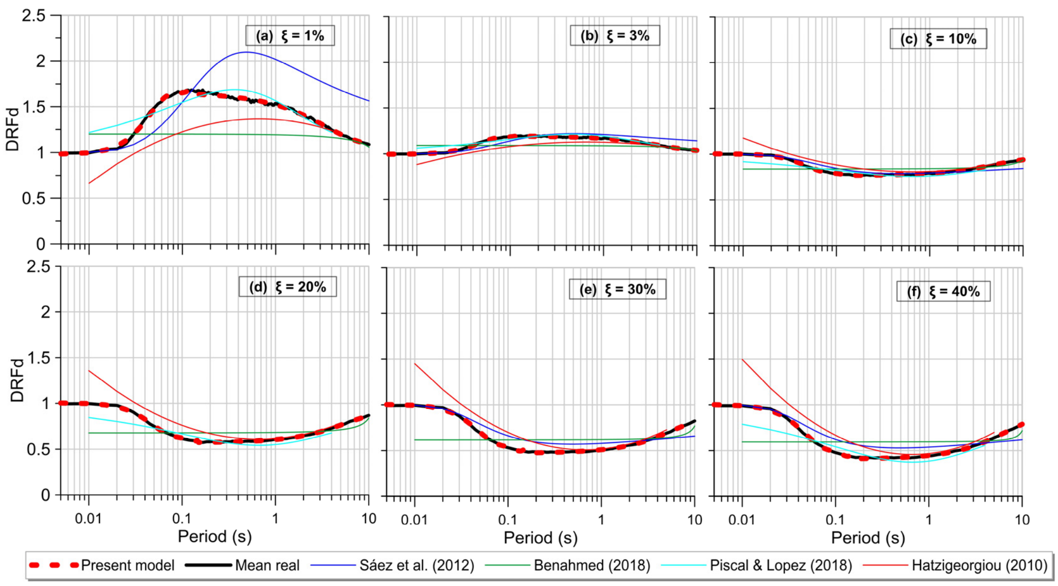

Figure 15. Comparison of proposed DRFd values with equations given in Table 5 [40,54–56] for different damping values.

It is also obvious from the figures that the Hatzigeorgiou [40] model does not fulfill the theoretical boundary restriction that the DRF should approach one as the natural vibration period approaches zero or infinity, and this may cause disparity [33]. In addition, this model was improved to account for the influence of the soil conditions and ground motion type (i.e., near- or far-fault earthquakes) as well as the effect of the damping ratio. It is also noteworthy that this model has relatively large errors when the natural vibration period is less than 0.5 s at all damping ratios. The predictions of the model for $T \leq 0.1$ s may not be comparable to the exact values since the model is valid for periods of $0.1 \text{ s} < T \leq 5.0$ s. In summary, the developed vertical DRFd model has precisely predicted the real DRFd values at all damping ratios and for the entire period range.

In Figure 16, the DRFv values predicted by the models from [33,40] are compared with the proposed model. It can be seen from the figure that for $\xi > 1\%$, all the models have good agreement between each other for natural periods greater than 0.1 s. The difference between the proposed model and the existing models is not particularly large, but the proposed model is still compatible with the real DRFv values determined from the analysis.

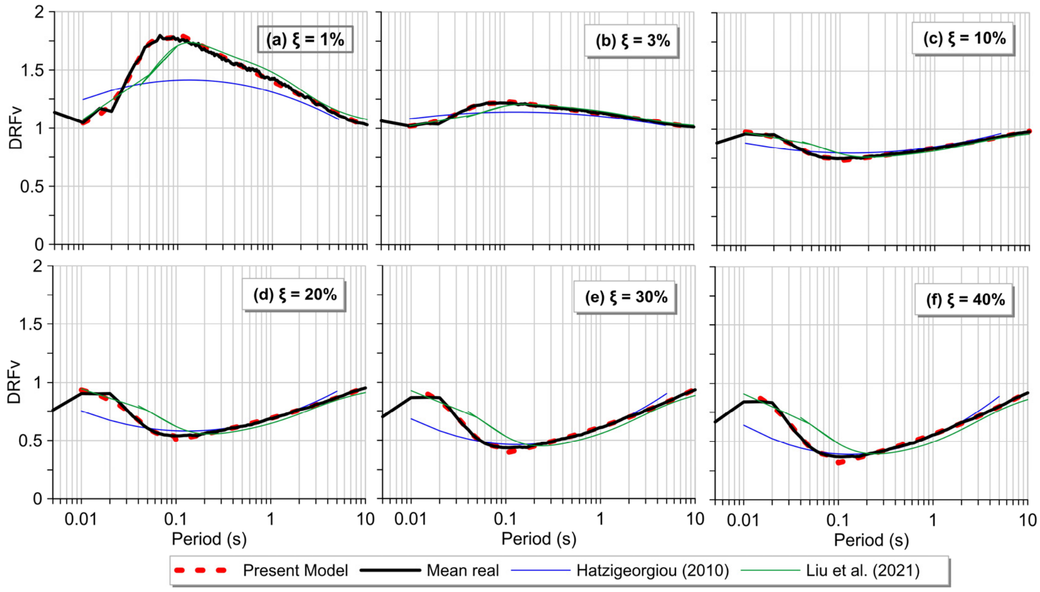

Figure 16. Comparison of proposed DRFv values with equations given in Table 5 [33,40] for different damping values.

5.3. Comparison with Seismic Codes

The DRFs defined in various modern seismic codes rely only on the damping values alone, and the natural period is not considered in the codes, as illustrated in the table earlier. Some developments in the DRFs were adopted in seismic codes, e.g., Newmark and Hall [41]'s equation was adopted in the ATC [57] and FEMA [58] codes, Bommer and Mendis [48]'s expression was approved in Eurocode 8 [13], and Ramirez et al. [59]'s formulation was adopted in FEMA 450 [60]. It also worth noting that the DRF equations recommended in the seismic codes are based on the horizontal response spectrum. However, the recent Kahramanmaraş earthquakes that occurred in Turkey have demonstrated that the vertical response spectrum of recorded motions can be also very high [61]. High vertical accelerations can be important for the design of seismically isolated structures since lateral movement is reduced by isolators, and non-structural elements in industrial facilities can reduce the seismic and economic losses. Assuming the DRF equations provided in the codes are valid in the vertical direction, Figure 17 compares the DRFs computed by the codes (given in Table 1) and the proposed model in this study for distinct natural vibration periods of 0.1 s, 0.25 s, 0.5 s, 1.0 s, and 2.0 s. Figure 17 indicates that the DRFs of the seismic codes [12–14,44–46] are compatible with the proposed model results for short periods (i.e., $T \leq 0.5$ s). On the other hand, the seismic codes diverge from the real DRFs and underestimate the DRF values with increasing periods and damping ratios.

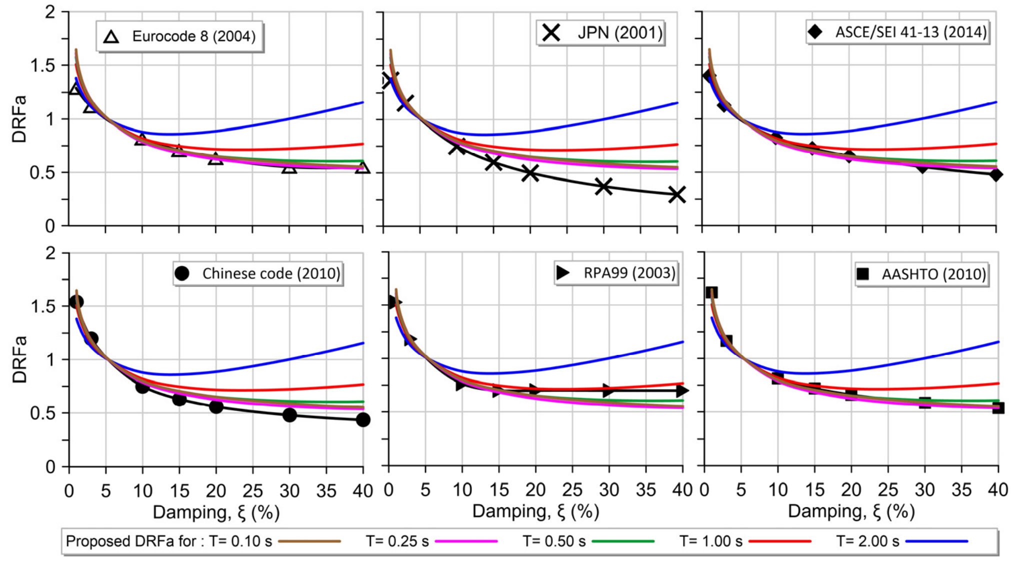

Figure 17. Comparison of proposed DRFa values and seismic codes [12–14,44–46] for different period values (T = 0.1; 0.25; 0.5; 1.0; and 2.0 s).

6. Conclusions

In this paper, the maximum displacement, relative velocity, and absolute acceleration response are calculated using the Newmark-β method to obtain the DRF values corresponding to different response spectrum types. Using 775 real vertical ground motions selected from the PEER database, each response spectrum was determined for damping ratios (ξ) of 1%, 3%, 5%, 10%, 15%, 20%, 30%, and 40%. Calculating the damping reduction values at damping ratios different from the 5% reference spectrum, namely the DRFa, DRFd, and DRFv, the effect of the earthquake magnitude (M_w), closest distance (R_{rup}), and site conditions was assessed. Based on these evaluations, new nonlinear prediction equations were developed for each response spectra using the damping ratio and the natural vibration period as variables. Consequently, the following conclusions could be drawn from the results:

1. The effect of the moment magnitude M_w on the DRFa is more pronounced than that on the DRFd and DRFv. Moreover, the effect of damping on the DRFa decreases with an increasing earthquake magnitude.
2. Compared to the DRFd and DRFv, the DRFa is less sensitive to the damping ratio for $R_{rup} > 30$ km.
3. The amplitude of and trend in the DRFs are relatively similar between the site classes A and D and B and C, respectively. It was observed that soil classes have no apparent effect on the DRFa at low damping ratios (1% and 3%). On the other hand, at high damping ratios, the soil classes influence the DRFa, especially for periods longer than 1.0 s.
4. The DRFs obtained from different spectra highlighted that DRFs based on displacement spectra and absolute acceleration spectra have the same trend and they can be described in similar functional form.
5. It was proven that the proposed equations for the DRFa, DRFd, and DRFv are strongly compatible with real DRFs and showed strong robustness when compared with the existing DRF models.
6. Comparison of the code recommendations with the proposed model revealed that they agree on the DRFa when $T \leq 0.5$ s. On the other hand, these seismic codes underestimate the DRFs for systems experiencing periods longer than 1.0 s.

Author Contributions: Conceptualization, B.B. and A.R.; methodology, A.R.; software, I.A.; validation, M.P., A.R. and I.A.; formal analysis, B.B.; investigation, A.R.; resources, A.R.; data curation, A.R.; writing—original draft preparation, A.R.; writing—review and editing, A.R., B.B., M.P. and I.A.; visualization, I.A.; supervision, B.B. All authors have read and agreed to the published version of the manuscript.

Funding: This research received no external funding.

Data Availability Statement: The authors offer their thanks to the Pacific Earthquake Engineering Research Center (PEER) ground motion database for providing the data.

Conflicts of Interest: The authors declare no conflicts of interest.

References

1. Abdollahiparsa, H.; Homami, P.; Khoshnoudian, F. Effect of Vertical Component of an Earthquake on Steel Frames Considering Soil-Structure Interaction. *KSCE J. Civ. Eng.* **2016**, *20*, 2790–2801. [CrossRef]
2. Moschen, L.; Medina, R.A.; Adam, C. Vertical Acceleration Demands on Column Lines of Steel Moment-resisting Frames. *Earthq. Eng. Struct. Dyn.* **2016**, *45*, 2039–2060. [CrossRef]
3. Gülerce, Z.; Abrahamson, N.A. Vector-Valued Probabilistic Seismic Hazard Assessment for the Effects of Vertical Ground Motions on the Seismic Response of Highway Bridges. *Earthq. Spectra* **2010**, *26*, 999–1016. [CrossRef]
4. Gulerce, Z.; Erduran, E.; Kunnath, S.K. Seismic Demand Models for Probabilistic Risk Analysis of near Fault Vertical Ground Motion Effects on Ordinary Highway Bridges. *Earthq. Eng. Struct. Dyn.* **2012**, *41*, 159–175. [CrossRef]
5. Mylonas, K. Vertical Response of Instrumented Structures. Ph.D. Thesis, Engineering Seismology and Earthquake Engineering Section, Imperial College, London, UK, 1997; 102p.
6. Mwafy, A.; Salah, A.; Elnashai, E. Vulnerability of Code-Compliant RC Buildings under Multi-Axial Earthquake Loading. In Proceedings of the International Conference on Earthquake Engineering, Taipei, Taiwan, 12–13 October 2006.
7. Kim, S.; Kim, S.J.; Chang, C. Analytical Assessment of the Effect of Vertical Ground Motion on RC Frames Designed for Gravity Loads with Various Geometric Configurations. *Adv. Civ. Eng.* **2018**, *2018*, 4029142. [CrossRef]
8. Bozorgnia, Y.; Niazi, M.; Campbell, K.W. Characteristics of Free-Field Vertical Ground Motion during the Northridge Earthquake. *Earthq. Spectra* **1995**, *11*, 515–525. [CrossRef]
9. Ambraseys, N.; Douglas, J. Near-Field Horizontal and Vertical Earthquake Ground Motions. *Soil Dyn. Earthq. Eng.* **2003**, *23*, 1–18. [CrossRef]
10. Campbell, K.W.; Bozorgnia, Y. Updated Near-Source Ground-Motion (Attenuation) Relations for the Horizontal and Vertical Components of Peak Ground Acceleration and Acceleration Response Spectra. *Bull. Seismol. Soc. Am.* **2003**, *93*, 314–331. [CrossRef]
11. Xinle, L.; Huijuan, D.; Xi, Z. Engineering Characteristics of Near-Fault Vertical Ground Motions and Their Effect on the Seismic Response of Bridges. *Earthq. Eng. Eng. Vib.* **2007**, *6*, 345–350.
12. *ASCE/SEI 41-13*; Seismic Evaluation and Retrofit of Existing Buildings. ASCE: Reston, VA, USA, 2014.
13. *Eurocode-8*; Eurocode 8: Design of Structures for Earthquake Resistance—Part 1: General Rules, Seismic Actions and Rules for Buildings. European Committee for Standardization: Brussels, Belgium, 2004; ISBN 0580458725.
14. *GB-2010*; Code for Seismic Design of Buildings. China Architecture and Building Press: Beijing, China, 2010.
15. *TBEC-2018*; Turkish Building Earthquake Code. Disaster and Emergency Management Presidency: Ankara, Turkiye, 2018.
16. Bozorgnia, Y.; Campbell, K.W. The Vertical-to-Horizontal Response Spectral Ratio and Tentative Procedures for Developing Simplified v/h and Vertical Design Spectra. *J. Earthq. Eng.* **2004**, *8*, 175–207. [CrossRef]
17. Setareh, M. Vibrations Due to Walking in a Long-Cantilevered Office Building Structure. *J. Perform. Constr. Facil.* **2012**, *26*, 255–270. [CrossRef]
18. Ye, J.-H.; Ding, Y.-L.; Liu, X.-M.; Huang, Z. Vibration Test and Analysis of An Aircraft Maintenance Hangar under Multi-Support Excitations. *Adv. Struct. Eng.* **2010**, *13*, 695–706. [CrossRef]
19. Davis, B.W.; Parnell, R.; Xu, L. Vibration Performance of Lightweight Floor Systems Supported by Cold-Formed Steel Joists. In Proceedings of the 19th International Specialty Conference on Recent Research and Developments in Cold-Formed Steel Design and Construction, St. Louis, MO, USA, 14–15 August 2008; pp. 325–339.
20. Varela, W.D.; Battista, R.C. Control of Vibrations Induced by People Walking on Large Span Composite Floor Decks. *Eng. Struct.* **2011**, *33*, 2485–2494. [CrossRef]
21. Zhou, Z.; Wong, J.; Mahin, S. Potentiality of Using Vertical and Three-Dimensional Isolation Systems in Nuclear Structures. *Nucl. Eng. Technol.* **2016**, *48*, 1237–1251. [CrossRef]
22. Kitayama, S.; Lee, D.; Constantinou, M.C.; Kempner, L. Probabilistic Seismic Assessment of Seismically Isolated Electrical Transformers Considering Vertical Isolation and Vertical Ground Motion. *Eng. Struct.* **2017**, *152*, 888–900. [CrossRef]
23. Xiang, Y.; Luo, Y.; Zhu, Z.; Shen, Z. Estimating the Response of Steel Structures Subjected to Vertical Seismic Excitation: Idealized Model and Inelastic Displacement Ratio. *Eng. Struct.* **2017**, *148*, 225–238. [CrossRef]

24. Xiang, Y.; Luo, Y.; Huang, Q.; Shen, Z. Vertical Ductility Demand and Residual Displacement of Roof-Type Steel Structures Subjected to Vertical Earthquake Ground Motions. *Soil Dyn. Earthq. Eng.* **2018**, *104*, 259–275. [CrossRef]
25. Mohraz, B. A Study of Earthquake Response Spectra for Different Geological Conditions. *Bull Seismol. Soc. Am.* **1976**, *66*, 915–935.
26. Trifunac, M.D.; Lee, V.W. Empirical Models for Scaling Pseudo Relative Velocity Spectra of Strong Earthquake Accelerations in Terms of Magnitude, Distance, Site Intensity and Recording Site Conditions. *Soil Dyn. Earthq. Eng.* **1989**, *8*, 126–144. [CrossRef]
27. Berge-Thierry, C.; Cotton, F.; Scotti, O.; Griot Pommera, D.-A.; Fukushima, Y. New Empirical Response Spectral Attenuation Laws for Moderate European Earthquakes. *J. Earthq. Eng.* **2003**, *7*, 193–222. [CrossRef]
28. Malhotra, P.K. Smooth Spectra of Horizontal and Vertical Ground Motions. *Bull. Seismol. Soc. Am.* **2006**, *96*, 506–518. [CrossRef]
29. Rezaeian, S.; Bozorgnia, Y.; Idriss, I.M.; Abrahamson, N.A.; Campbell, K.W.; Silva, W.J. Damping Scaling Factors for Vertical Elastic Response Spectra for Shallow Crustal Earthquakes in Active Tectonic Regions. *Earthq. Spectra* **2014**, *30*, 1335–1358. [CrossRef]
30. Akkar, S.; Sandıkkaya, M.A.; Ay, B.Ö. Compatible Ground-Motion Prediction Equations for Damping Scaling Factors and Vertical-to-Horizontal Spectral Amplitude Ratios for the Broader Europe Region. *Bull. Earthq. Eng.* **2014**, *12*, 517–547. [CrossRef]
31. Akkar, S.; Sandıkkaya, M.A.; Bommer, J.J. Empirical Ground-Motion Models for Point- and Extended-Source Crustal Earthquake Scenarios in Europe and the Middle East. *Bull. Earthq. Eng.* **2014**, *12*, 359–387. [CrossRef]
32. Xiang, Y.; Huang, Q.L. Damping Modification Factor for the Vertical Seismic Response Spectrum: A Study Based on Japanese Earthquake Records. *Eng. Struct.* **2019**, *179*, 493–511. [CrossRef]
33. Liu, T.; Wang, W.; Wang, H.; Su, B. Improved Damping Reduction Factor Models for Different Response Spectra. *Eng. Struct.* **2021**, *246*, 113012. [CrossRef]
34. Zhang, H.; Zhao, Y. Damping Modification Factor Based on Random Vibration Theory Using a Source-Based Ground-Motion Model. *Soil Dyn. Earthq. Eng.* **2020**, *136*, 106225. [CrossRef]
35. Elhout, E.A. Damping Modification Factor of the Vertical Response Spectrum. *Asian J. Civ. Eng.* **2022**, *23*, 929–942. [CrossRef]
36. Hu, J.; Liu, M.; Tan, J. Damping Modification Factors for Horizontal and Vertical Acceleration Spectra from Offshore Ground Motions in the Japan Sagami Bay Region. *Bull. Seismol. Soc. Am.* **2022**, *112*, 2621–2641. [CrossRef]
37. Çelik, E.Ç.; Merter, O. An Investigation of Damping Modification Factors Corresponding to Different Damping Ratios for Sdof Systems. *Stavební Obz.—Civ. Eng. J.* **2023**, *32*, 42–53. [CrossRef]
38. Sriwastav, R.K.; Basu, D. Simplified Damping Modification Factor for Vertical Response Spectra. In *Symposium in Earthquake Engineering*; Shrikhande, M., Agarwal, P., Kumar, P.C.A., Eds.; Lecture Notes in Civil Engineering; Springer Nature: Singapore, 2023; Volume 332 LNCE, pp. 655–667; ISBN 9789819914586.
39. Baizid, B.; Cardone, D. Estimation of Stochastic Damping Reduction Factor Using Monte Carlo Simulation and Artificial Neural Network Method. *Ing. Sismica* **2021**, *38*, 37–53.
40. Hatzigeorgiou, G.D. Damping Modification Factors for SDOF Systems Subjected to Near-Fault, Far-Fault and Artificial Earthquakes. *Earthq. Eng. Struct. Dyn.* **2010**, *39*, 1239–1258. [CrossRef]
41. Newmark, N.M.; Hall, W.J. Procedures and Criteria for Earthquake Resistant Design. In *Building Practices for Disaster Mitigation*; Building Science Series 46; National Bureau of Standards: Reston, VA, USA, 1972; pp. 209–236.
42. Dávalos, H.; Miranda, E.; Bantis, J.; Cruz, C. Response Spectral Damping Modification Factors for Structures Built on Soft Soils. *Soil Dyn. Earthq. Eng.* **2022**, *154*, 107153. [CrossRef]
43. *NTC-2018*; New Technical Standards for Buildings. Ministero delle Infrastrutture e dei Trasporti: Roma, Italy, 2018. (In Italian)
44. *JPN Guidelines for Calculation Procedure and Technical Standard on Seismically Isolated Structures*; Building Center of Japan: Tokyo, Japan, 2001. (In Japanese)
45. AASHTO. *LFRD Bridge Design Specifications*, 3rd ed.; American Association of State Highway and Transportation Officials: Washington, DC, USA, 2010.
46. *RPA99*; Algerian Earthquake Resistant Regulations. National Center of Applied Research in Earthquake Engineering: Algiers, Algeria, 2003.
47. Ancheta, T.D.; Darragh, R.B.; Stewart, J.P.; Seyhan, E.; Silva, W.J.; Chiou, B.S.-J.S.J.; Wooddell, K.E.; Graves, R.W.; Kottke, A.R.; Boore, D.M.; et al. NGA-West2 Database. *Earthq. Spectra* **2014**, *30*, 989–1005. [CrossRef]
48. Bommer, J.J.; Mendis, R. Scaling of Spectral Displacement Ordinates with Damping Ratios. *Earthq. Eng. Struct. Dyn.* **2005**, *34*, 145–165. [CrossRef]
49. Cauzzi, C.; Faccioli, E. Broadband (0.05 to 20 s) Prediction of Displacement Response Spectra Based on Worldwide Digital Records. *J. Seismol.* **2008**, *12*, 453–475. [CrossRef]
50. Sriwastav, R.K.; Basu, D. Characterisation of Design Spectra for Vertical Ground Motion. *Int. J. Earthq. Impact Eng.* **2022**, *4*, 1–29. [CrossRef]
51. Palanci, M. Flexural Response Prediction of Reinforced Concrete Members Based on Statistical Observations. *Arab. J. Sci. Eng.* **2017**, *42*, 3689–3709. [CrossRef]
52. Benahmed, B.; Hammoutene, M.; Cardone, D. Effects of Damping Uncertainties on Damping Reduction Factors. *Period. Polytech. Civ. Eng.* **2016**, *61*, 341. [CrossRef]
53. Lin, Y.; Chang, K. Effects of Site Classes on Damping Reduction Factors. *J. Struct. Eng.* **2004**, *130*, 1667–1675. [CrossRef]
54. Piscal, A.C.M.; López-Almansa, F. Generating Damping Modification Factors after Artificial Inputs in Scenarios of Local Records Scarcity. *Bull. Earthq. Eng.* **2018**, *16*, 5371–5396. [CrossRef]

55. Benahmed, B. Formulation of Damping Reduction Factor for the Algerian Seismic Code. *Asian J. Civ. Eng.* **2018**, *19*, 375–385. [CrossRef]
56. Sáez, A.; Moroni, M.O.; Sarrazin, M. Contributions to the Chilean Code for Seismic Design of Buildings with Energy Dissipation Devices. In Proceedings of the 15th World Conference on Earthquake Engineering, Lisbon, Portugal, 24–28 September 2012.
57. *ATC-40*; Seismic Evaluation and Retrofit of Concrete Buildings. Applied Technology Council: Redwood City, CA, USA, 1996.
58. *FEMA 440*; Improvement of Nonlinear Static Seismic Analysis Procedures. Federal Emergency Management Agency: Redwood City, CA, USA, 2015; ISBN 978-1484019436.
59. Ramirez, O.M.; Constantinou, M.C.; Whittaker, A.S.; Kircher, C.A.; Chrysostomou, C.Z. Elastic and Inelastic Seismic Response of Buildings with Damping Systems. *Earthq. Spectra* **2002**, *18*, 531–547. [CrossRef]
60. *FEMA 450*; NEHRP Recommended Provisions for Seismic Regulations for New Buildings and Other Structures. Building Seismic Safety Council: Washington DC, USA, 2003.
61. Senel, S.M.; Kayhan, A.H.; Palanci, M.; Demir, A. Assessment of Damages in Precast Industrial Buildings in the Aftermath of Pazarcık and Elbistan Earthquakes. *J. Earthq. Eng.* **2024**, 1–30. [CrossRef]